Dalton Transactions

Accepted Manuscript

ROYAL SOCIETY OF CHEMISTRY

www.rsc.org/dalton

Meso enyne substituted BODIPYs: synthesis, structure and properties

Bhausaheb Dhokale, Thaksen Jadhav, Shaikh M. Mobin and Rajneesh Misra*

Department of Chemistry, Indian Institute of Technology Indore 452 017 (India)

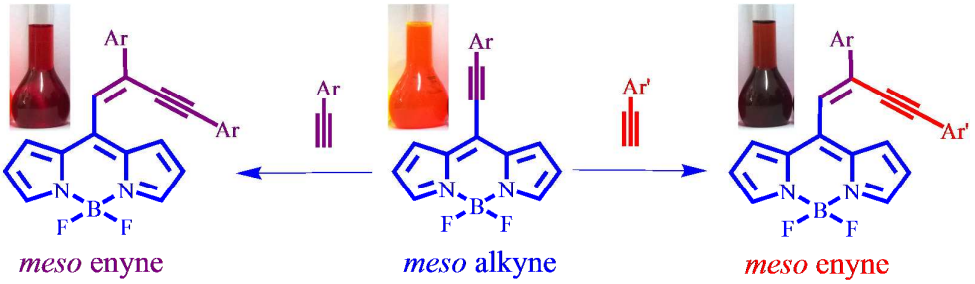

ABSTRACT

We report the synthesis of *meso* enyne substituted BODIPYs by the reaction of 8-chloro BODIPY with terminal alkynes under Sonogashira coupling condition, and by Pd-Cu catalyzed hydroalkynylation reaction of terminal alkynes, across the –C≡C– bond of *meso* alkynylated BODIPYs. The scope of reaction was explored by reacting different *meso* alkynylated BODIPYs with various terminal alkynes, which results *meso* enyne substituted BODIPYs with different substituents. The *meso* enyne substituted BODIPYs show blue shifted absorption and red shifted emission with large Stokes shift compared to *meso* alkynylated BODIPYs. The single crystal structure of BODIPYs **2a**, **3b**, **4a** and **2d** are reported. Their packing diagram exhibits extensive intermolecular C-H---π, C-H---F hydrogen bonding and π---π staking interaction, leading to 1D supramolecular frameworks extending into the complex 3D structural frameworks.

INTRODUCTION

The BODIPY fluorophore outdistances itself from contemporary fluorophores, due to its unique photophysical properties such as strong absorption with high molar extinction coefficient and high fluorescence quantum yield.[1] The BODIPY dyes have been explored for variety of applications such as ion sensing, non-linear optics, organic photovoltaics, photodynamic therapy and bio-medical imaging.[2] The photonic properties of the BODIPY fluorophore can be tuned by introducing the appropriate functionalities at α, β and *meso* positions or by ring-fusion.[3] The *meso* alkynylated BODIPYs exhibit red shifted absorption than α and β-alkynylated BODIPYs, but their absorption is blue shifted than α-alkynylated benzo-fused BODIPYs.[4]

Our group is involved in the design and synthesis of donor substituted, β and *meso* functionalized BODIPYs for optoelectronic applications.[5] Recently we reported the synthesis of *meso* enamine substituted BODIPYs by catalyst free oxidation of *tert*-amines and cross coupling with 8-chloro BODIPY.[6]

Enynes are important building block in synthetic chemistry, and has been explored in organic electronics.[7] The literature reveals formation of enynes as side product in Sonogashira coupling reaction of certain aryl halides with terminal alkynes.[8] There are few reports, where enynes were obtained as major product.[9] Tremendous efforts have been devoted for the selective synthesis of *E* or *Z* enynes by metal catalyzed alkyne dimerization.[10]

Herein we report the synthesis of *meso* enyne substituted BODIPYs by reacting excess terminal alkynes with 8-chloro BODIPY under Sonogashira coupling condition (Method A), and by the Pd-Cu catalyzed hydroalkynylation reaction of terminal alkynes across the –C≡C– bond of *meso* alkynylated BODIPY (Method B) and their structural, photophysical and electrochemical properties. The reaction methodology furnishes, *meso* enyne substituted BODIPYs in good yields with two different substituents at a time. The

methodology involves Pd-Cu catalyzed –C≡C– bond activation and new C–C bond formation.

Results and Discussion

The reaction of 8-chloro BODIPY **1**, with excess terminal alkynes **a** and **b** under Sonogashira coupling condition resulted BODIPYs **2a** and **2b** as major products in 58 % and 57 % yields along with minor products **3a** and **3b** in 20 % and 21 % yields respectively (Method A; Scheme 1).

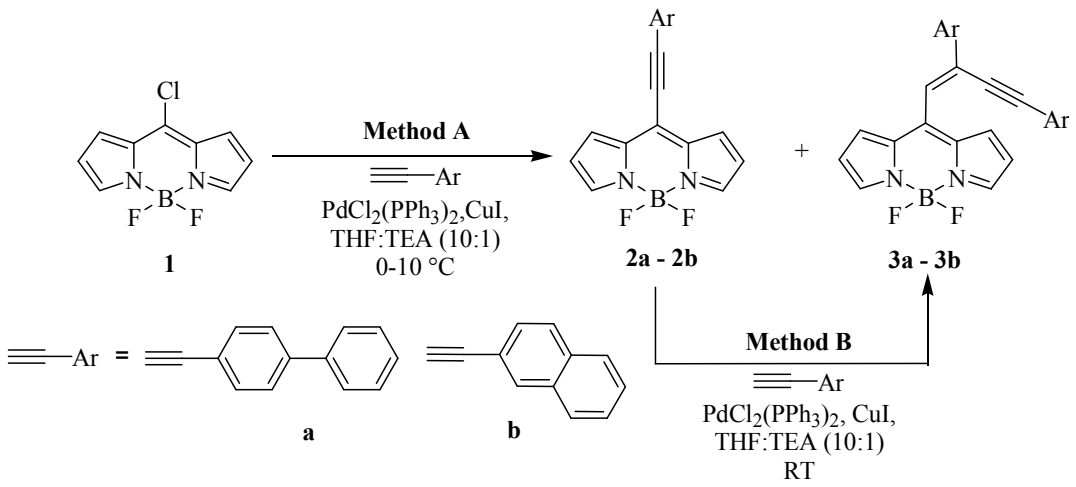

Scheme 1 Synthesis of *meso* ethynyl and enyne substituted BODIPYs **2a**, **2b** and **3a**, **3b**.

The isolated *meso* alkynylated BODIPYs **2a** and **2b** were subjected to Pd-Cu catalyzed hydroalkynylation reaction with alkynes **a** and **b**, which resulted *meso* enyne substituted BODIPYs **3a** and **3b** in 60 % and 62 % yield respectively (Method B; Scheme 1). The reaction works well in different solvents like tetrahydrofuran, toluene and dichloromethane, but presence of both $Pd(PPh_3)_2Cl_2$ and CuI catalysts are essential for the reaction.

The scope of the reaction was explored to incorporate two different substituents into the BODIPY. The *meso* alkynylated BODIPYs **2a – 2c** were subjected to Pd-Cu catalyzed hydroalkynylation reaction with ethynyl ferrocene (Scheme 2), which resulted *meso* enyne substituted BODIPYs **4a**, **4b** and **4c** in 61 %, 60 % and 58 % yields respectively.

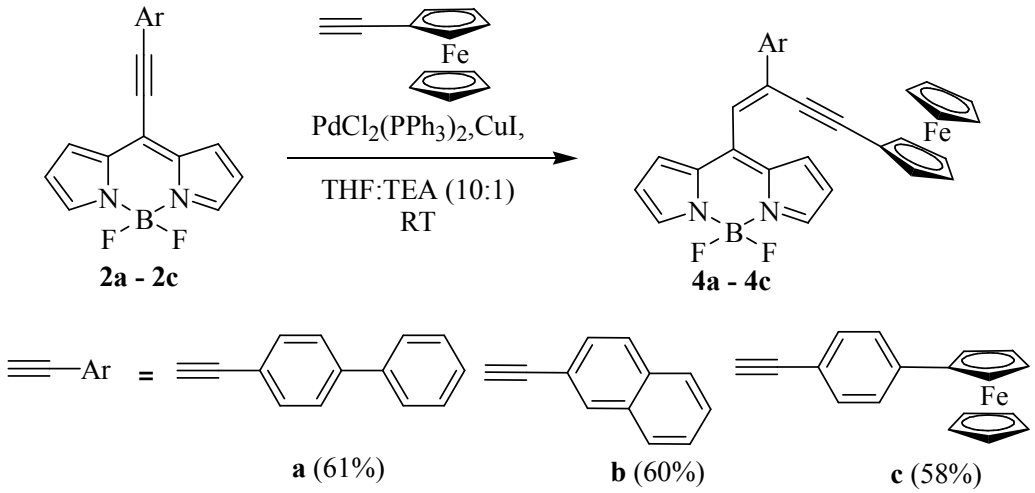

Scheme 2 Synthesis of *meso* ferrocenyl enyne substituted BODIPYs **4a – 4c** (Isolated yields in bracket).

The scope of the reaction was further explored for the Stille coupling. We tried the Stille reaction of (Phenylethynyl)tributylstannane with the 8-chloro BODIPY. The reaction resulted only *meso* alkynylated BODIPY **2d** in 80 % yield (Scheme 3). Even use of excess (Phenylethynyl)tributylstannane in Stille reaction resulted only BODIPY **2d**.[11]

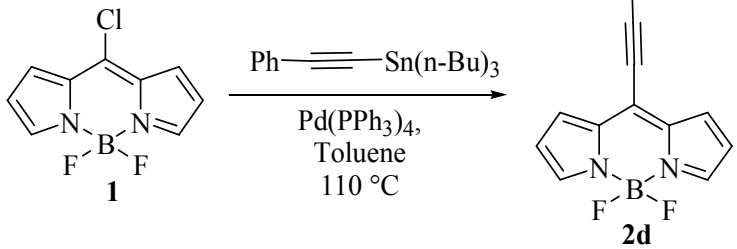

Scheme 3 Synthesis of BODIPY **2d** by Stille reaction.

The plausible mechanism for the Pd-Cu catalyzed hydroalkynylation reaction across the –C≡C– of *meso* alkynylated BODIPYs is displayed in Scheme 4. The coordination of $Pd^{[0]}$ species with the –C≡C– bond of *meso* alkynylated BODIPY results π-complex **A**. The activation of the terminal alkyne by Cu results σ-complex **B**. The combination of **A** and **B** leads to the intermediate **C**, which further transforms into the *meso* alkynylated BODIPY.[12]

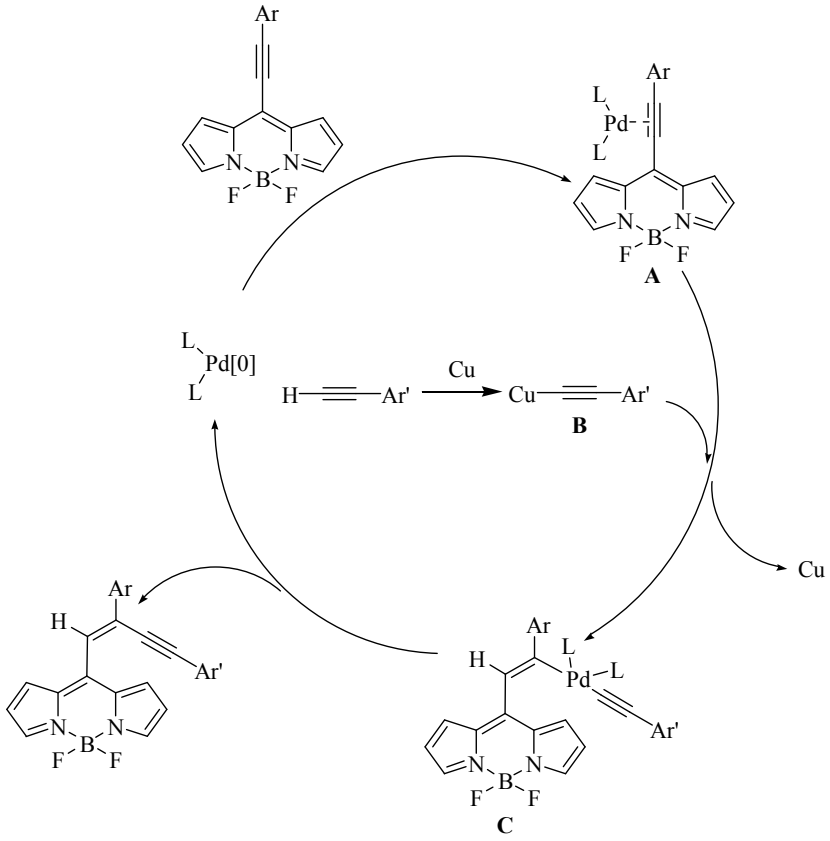

Scheme 4 Plausible reaction mechanism.

The BODIPYs were well characterized by ^{1}H NMR, ^{13}C NMR and HRMS techniques. The BODIPYs **2a**, **3b**, **4a** and **2d** were also characterized by single crystal X-ray crystallography.

PHOTOPHYSICAL PROPERTIES

The electronic absorption and emission spectra of the BODIPYs **1 – 4** were recorded in toluene (Fig. 1 and S1 – S3; ESI) and the corresponding data are displayed in Table 1. The color variations in the BODIPY solution are shown in Fig. 2. The *meso* alkynylated BODIPYs **2a** – **2c** exhibit absorption band at ~ 548 nm. The electronic absorption spectrum of *meso* enyne substituted BODIPYs **3a** and **3b** exhibits blue shift of ~ 34 nm compared to the *meso* alkynylated BODIPYs **2a – 2c** due to the loss of planarity between enyne substituent and BODIPY (torsional angle from crystal structure 50.60°).

The ferrocenyl enyne substituted BODIPYs **4a** – **4c** exhibit blue shift of ~ 38 nm, which suggests that incorporation of bulkier alkyne (ethynyl ferrocene) disturbs the planarity more than the BODIPYs **3a – 3c** (torsional angle from crystal structure 58.41°).

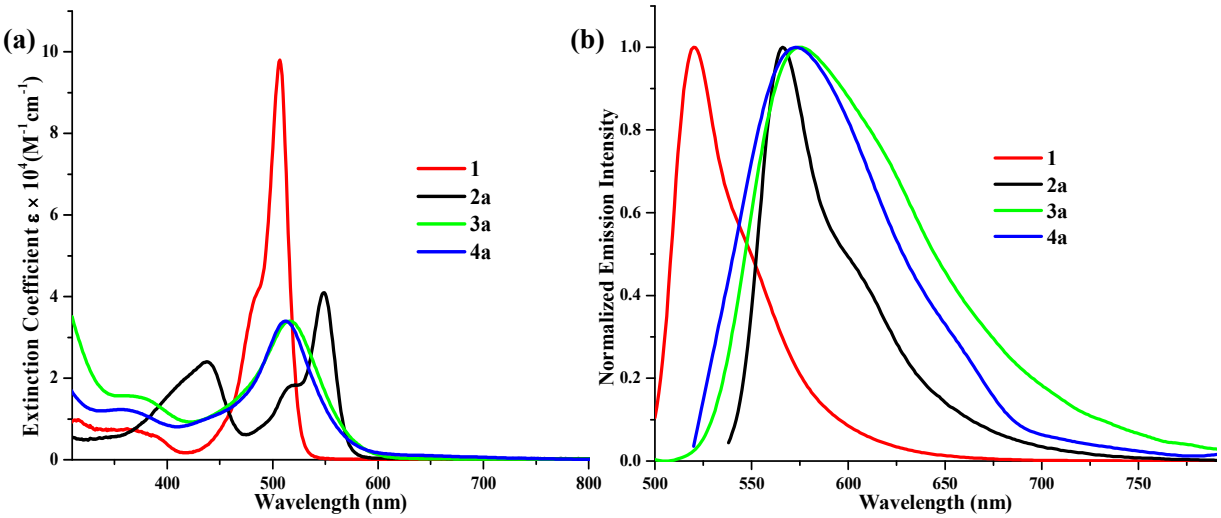

Fig. 1 (a) Electronic absorption spectra and (b) Normalized emission spectra of BODIPYs **1**, **2a**, **3a** and **4a** in toluene at the concentration of 0.1 optical densities at λ_{max}.

The *meso* alkynylated BODIPYs **2a** and **2b** exhibits sharp emission band at ~ 566 nm whereas, the *meso* enyne substituted BODIPYs **3a** and **3b** exhibit ~ 8 nm red shifted broad emission band with lower quantum yield. (Fig. 1 (b) and S3 (ESI); Table 1). The decrease in fluorescence quantum yield can be attributed to the dissipation of excited state energy by increased molecular rotations.[13] The BODIPYs bearing ferrocenyl unit (**4a – 4c**) are poorly emissive in nature due to the fast non-radiative deactivation of the exited state with intramolecular charge transfer from the donor ferrocenyl unit to the acceptor BODIPY moiety.[14]

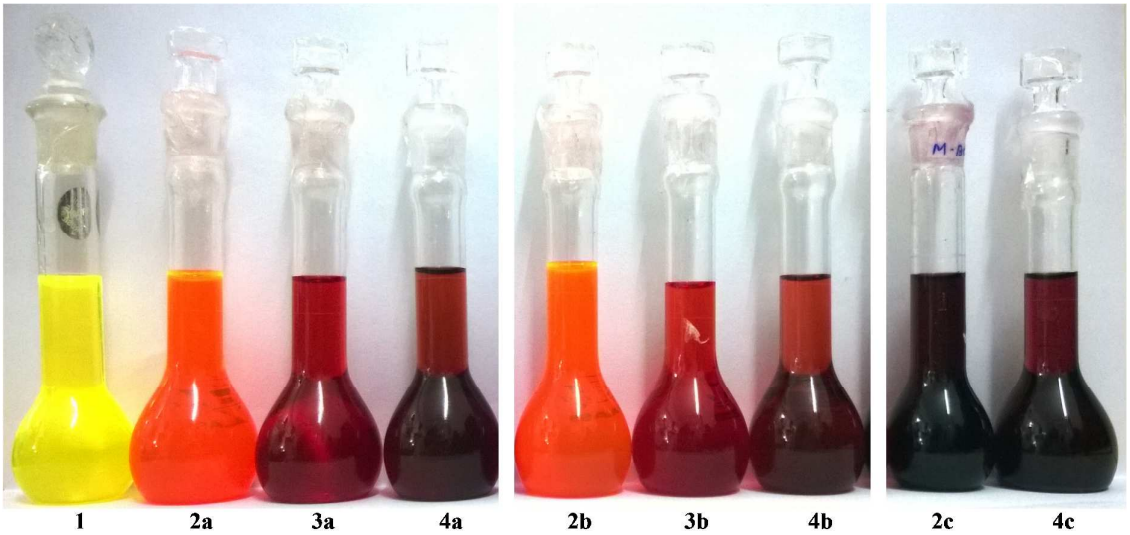

Fig. 2 BODIPYs **1 – 4** in Toluene at 10^{-4} M concentration.

The *meso* alkynylated BODIPYs **2a**, **2b** and **2c** exhibit Stokes shift of 500 – 600 cm^{-1}, whereas the *meso* enyne substituted BODIPYs **3a**, **3b**, **4a** and **4b** exhibit Stokes shift of ~ 2000 cm^{-1}. The large Stokes shift of enyne substituted BODIPYs can be attributed to the higher differences in the excited state dipole moment and free molecular rotations.[13] The absorption and emission spectra of the BODIPYs were recorded in different solvents. The absorption spectra of BODIPYs **2 – 4** show blue shift in polar solvents and red shift in non polar solvents (Fig. S4 – S9), which indicates the negative solvatochromic effect.

Table 1 Photophysical properties of BODIPYs **2 – 4**.

BODIPY	**λ_{max} (nm)**	**$\varepsilon \times 10^4$ ($M^{-1}.cm^{-1}$) [a]**	**λ_{em} [b] (nm)**	**Stokes shift (cm^{-1})**	**Φ_F [c]**
2a	548	4.1	566	580	0.50
2b	549	4.2	567	578	0.43
3a	515	3.4	575	2026	0.05
3b	515	3.6	575	2026	0.04
4a	510	3.4	572	1940	0.0001
4b	510	3.5	568	2095	0.0004
4c	511	3.7	–[d]	–	–

[a]Recorded at $\lambda_{max,}$ [b]Excited at $\lambda_{max,}$ [c]Determined by using Rhodamine 6G as standard (ϕ = 0.88, in ethanol), [d]BODIPYs are non-emissive in nature

ELECTROCHEMICAL PROPERTIES

The electrochemical properties of BODIPYs **2** – **4** were investigated by cyclic and differential pulse voltammetric (CV and DPV) techniques in a 0.1 M solution of Bu_4NPF_6 in dichloromethane at 100 mVs^{-1} scan rate, versus Fc/Fc^+ (Fig. 3 and S10 – S13). The electrochemical data are displayed in Table 2. The redox waves of the BODIPY origin are irreversible, whereas the ferrocenyl oxidation waves are reversible in nature (dotted blue line; Fig. 3).

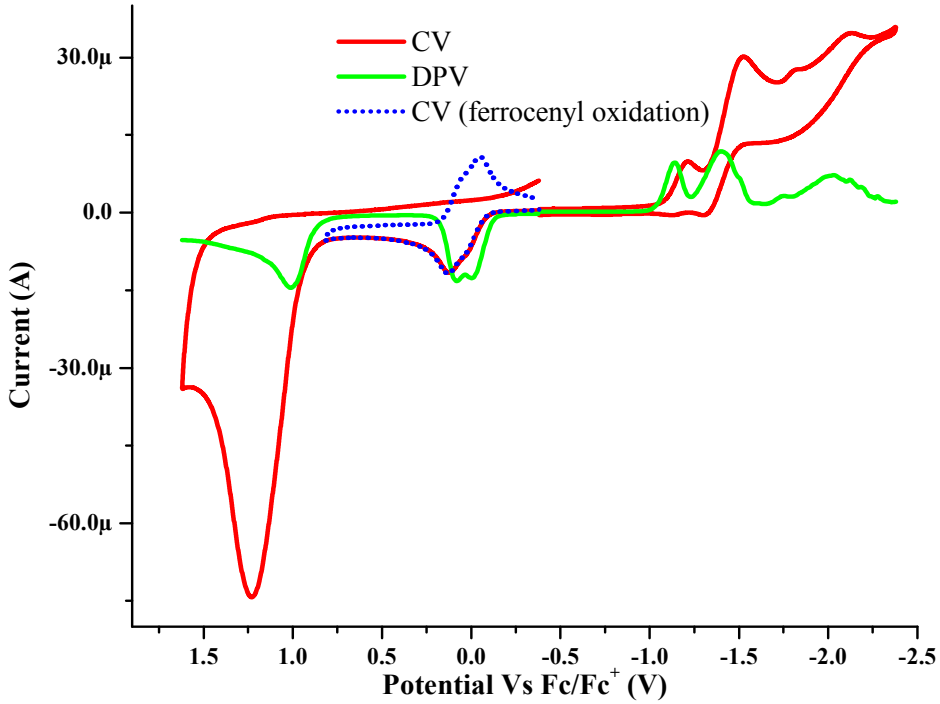

Fig. 3 Overlaid CV and DPV plots of *meso* enyne substituted BODIPY **4c** bearing two ferrocenyl units in different environment.

The first reduction potential follows the order **2a>3a>4a** (Table 2), indicating better delocalization of donor electrons onto the BODIPY moiety in *meso* enyne substituted BODIPYs compared to *meso* alkynylated BODIPYs. The harder reduction of BODIPY **4** compared to BODIPY **3** indicates better electron donating ability of ferrocene than biphenyl and naphthalene moieties.

The BODIPY **4c** exhibits two merging oxidation waves in CV and DPV at 0.08 V and 0.00 V, corresponding to the oxidation of ferrocenyl moiety attached to the triple bond and the phenyl ring respectively.

Table 2 The electrochemical properties of the BODIPYs **2 – 4.**

BODIPY	E^2 Oxid[b] (BODIPY)	E^1 Oxid[b] (BODIPY)	E^1 Oxid (Fc)	E^1 Red[b] (BODIPY)	E^2 Red[b] (BODIPY)
2a	1.35	1.10	-	-0.98	-1.35
2b	1.28	1.07	-	-0.99	-1.28
3a	1.41	1.01	-	-1.04	-1.36
3b	1.33	0.97	-	-1.08	-1.41
4a	-	1.16	0.10	-1.12	-1.40
4b	-	1.17	0.08	-1.13	-1.43
4c	-	1.01	0.00 (Phenyl Fc) 0.08 (Ethynyl Fc)	-1.14	-1.40

[a]The electrochemical analysis was performed in a 0.1 M solution of Bu_4NPF_6 in dichloromethane at 100 mVs^{-1} scan rate, versus Fc/Fc^+. [b]Irreversible wave.

THEORETICAL CALCULATIONS

Computational calculation was performed using density functional theory (DFT), and the frontier molecular orbitals (FMOs) of the BODIPYs **2 – 4** are displayed in Fig. 4 and S22 (ESI). The LUMO in BODIPYs **2a**, **3a** and **4a** are localized on the BODIPY core, which indicates the strong acceptor nature of BODIPY. The HOMO in **2a** is distributed on BODIPY and in **3a** on BODIPY as well as on the ethynyl biphenyl moiety, indicating better electronic distribution. The HOMO in BODIPYs **4a** is localized on the ferrocenyl part only due to the stronger electron donating ability of ethynyl ferrocene than ethynyl biphenyl. The overall distribution of HOMO on aryl moiety and LUMO on BODIPY reflects the strong donor acceptor interactions in *meso* enyne substituted BODIPYs.

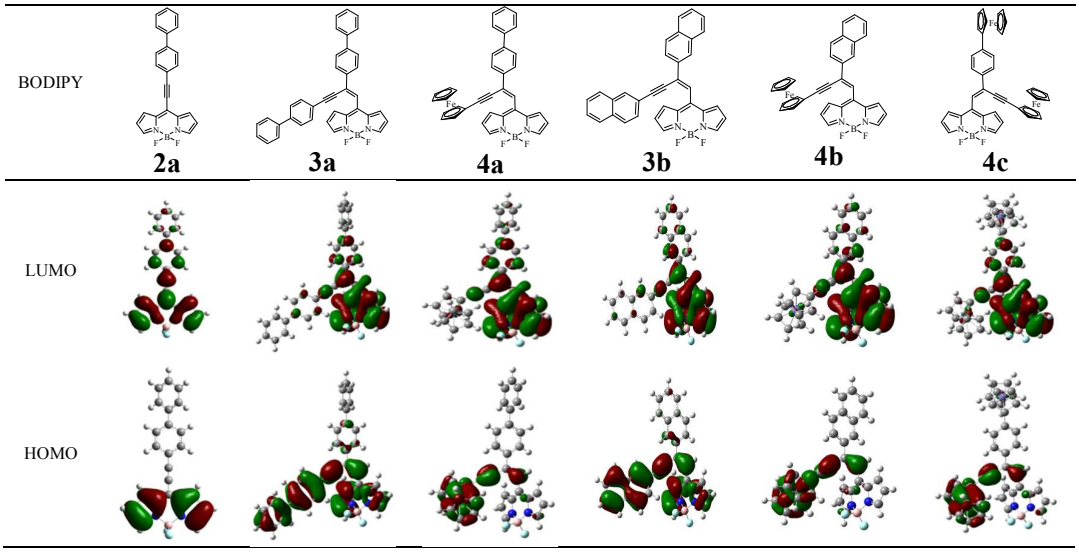

Fig. 4 Frontier molecular orbital plots of BODIPYs **2 – 4**, calculated at B3LYP/6-31G* level for C, N, B, F, H, and Lanl2DZ level for Fe.

CRYSTAL STRUCTURE

The Single crystals of the BODIPYs **2a**, **3b**, **4a** and **2d** were obtained by slow evaporation of their dichloromethane:hexane solution at room temperature. The BODIPY **2a** crystalizes into monoclinic *C*2/c space group, **3b** and **4a** crystallizes into triclinic *P*-1 space group, whereas the BODIPY **2d** crystallizes into monoclinic $P2_1/c$ space group. The crystal structure and data refinement parameters are displayed in Table S2 (ESI). The crystal structures reveal that the *meso* enyne substituted BODIPYs were obtained only in (*E*) conformation. The highly planar BODIPY core in *meso* alkynylated BODIPYs maintains planarity in *meso* alkynylated BODIPYs also (Fig. 5).

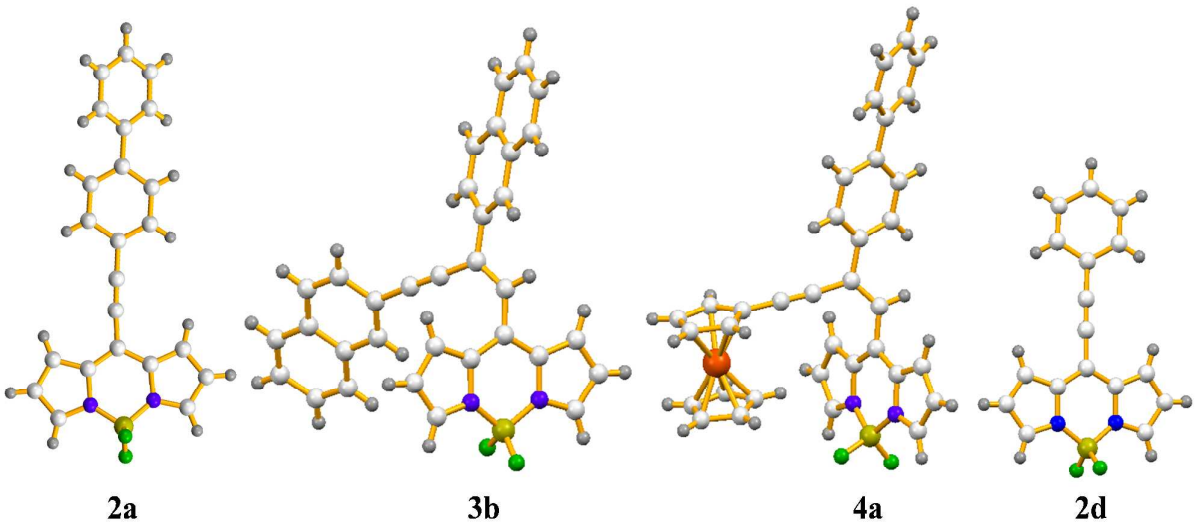

Fig. 5 Single crystal structures of BODIPYs **2a**, **3b**, **4a** and **2d** (BODIPY **2a**: Only molecule B is shown from the asymmetric unit; details in Fig. S14; ESI).

The comparison of selected bond lengths and bond angles of the crystal structure is shown in Figure S20 and S21 (ISI) respectively. The *meso* substituent and BODIPY core are planar in *meso* alkynylated BODIPYs, and non-planar in *meso* enyne substituted BODIPYs. The higher torsional angle between BODIPY plane and *meso* enyne substituent in BODIPY **4a** than BODIPY **3b**, suggests the bulky nature of ferrocenyl moiety than naphthalene moiety, which supports the higher blue shit in the absorption spectra of **4a** and **4b** than **3a** and **3b**.

The close packing in the crystal structures of BODIPYs **2a**, **3b**, **4a** and **2d** exhibit marvelous supramolecular frameworks. The distances and angles of the supramolecular interactions in the crystals are shown in Table 3.

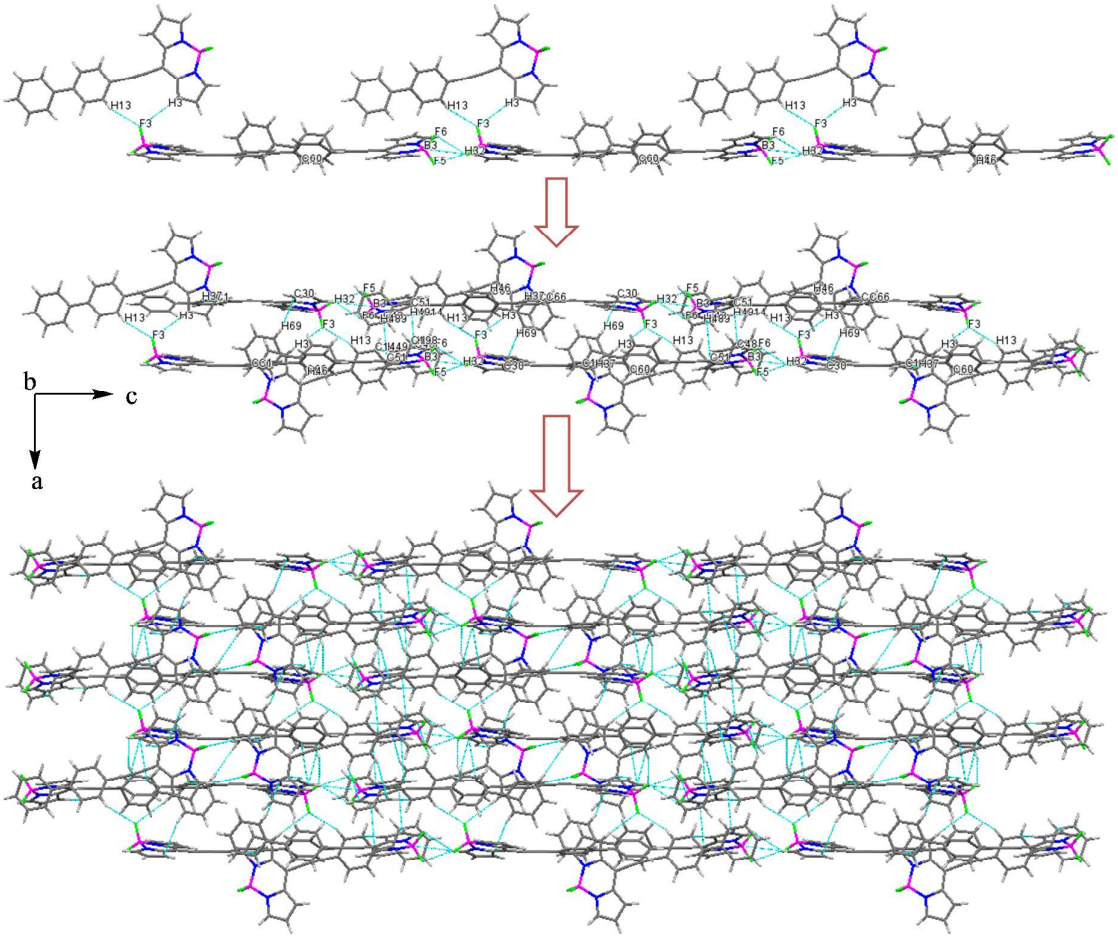

Fig. 6 Crystal structure packing of BODIPY **2a**.

The crystal structure of BODIPY **2a** contains three molecules (A, B and C) in an asymmetric unit. These three molecules slightly differ in bond lengths and angles. The C(46)-H(46)---π (Phenyl) interaction connects molecule B and C whereas the (13)-H(13)---F(3) and C(3)-H(3)---F(3) interactions connect molecules B and A. The molecules B and C form a chain along *c*-axis with molecule A hanging above the chain with C(32)-H(32)---F(6) and C(32)-H(32)---F(5) interactions. The two chains are arranged in antiparallel fashion via π---π stacking interaction between two pyrrolic rings of molecule C. The set of two antiparallel chains further grows into a complex 3D framework via C(1)-H(1)---F(1), C(59)-H(59)---F(4), C(16)-H(16)---π (Pyrrolic), C(17)-H(17)---π (Pyrrolic) and C(31)-H(31)---π (Pyrrolic) interactions (Fig. 6).

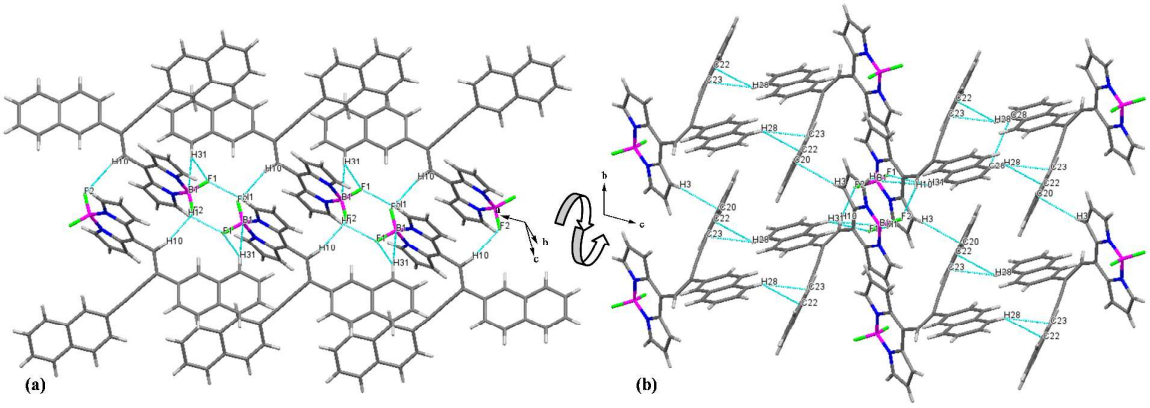

Fig. 7 Crystal structure packing of BODIPY **3b**.

In the packing diagram of BODIPY **3b**, the two molecules form a dimeric structure in head to head sliding manner via two mutual C(10)-H(10)---F(2) interactions. These dimers connect to one-another diagonally to form a 1D chain along *a*-axis via C(31)-H(31)---F(1) and C(1)-H(1)---F(1) interactions (Fig. 7(a)). These one dimensional chains connect to another chains laterally via C(3)-H(3)---π and C(28)-H(28)---π interactions along *b* and *c* axis respectively to form complex 3D framework (Fig. 7(b)).

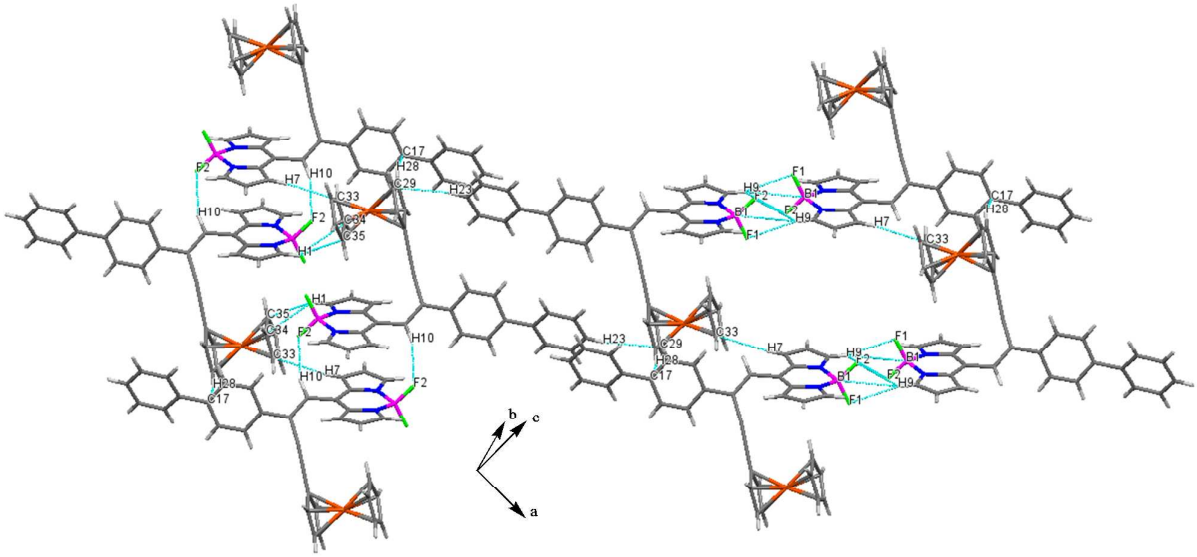

Fig. 8 Crystal structure packing of BODIPY **4a**.

Table 3 Distances and angles of intermolecular interactions in the crystal structures of BODIPYs **2a**, **3b**, **4a** and **2d**.

Sr. No.	Interaction	Distance (Å)	Angle (°)
	BODIPY **2a**		
1	C(1)-H(1)---F(1)	2.504	147.10
2	C(3)-H(3)---F(3)	2.588	172.52
3	C(13)-H(13)---F(3)	2.527	147.56
4	C(59)-H(59)---F(4)	2.402	158.47
5	C(32)-H(32)---F(5)	2.413	155.87
6	C(32)-H(32)---F(6)	2.597	150.25
7	C(16)-H(16)---π (Pyrrolic)	2.481	
8	C(17)-H(17)---π (Pyrrolic)	3.277	
9	C(31)-H(31)---π (Pyrrolic)	3.093	
10	C(25)-H(25)---π (Pyrrolic)	2.892	
11	C(46)-H(46)---π (Phenyl)	3.606	
	BODIPY **3b**		
1	C(31)-H(31)---F(1)	2.638	145.99
2	C(1)-H(1)---F(1)	2.354	164.33
3	C(10)-H(10)---F(2)	2.493	165.23
4	C(3)-H(3)---π (Naph)	3.183	
5	C(28)-H(28)---π (Naph)	2.733	
	BODIPY**4a**		
1	C(9)-H(9)---F(1)	2.664	161.46
2	C(9)-H(9)---F(2)	2.645	147.39
3	C(10)-H(10)---F(2)	2.324	153.72
4	C(1)-H(1)---π (Fc)	3.183	
5	C(7)-H(7)---π (Fc)	3.395	
6	C(28)-H(28)---π (Phenyl)	3.271	
7	C(23)-H(23)---π (Fc)	2.731	
	BODIPY **2d**		
1	C(1)-H(1)---F(1)	2.397	160.15
2	C(8)-H(8)---F(2)	2.570	153.85
3	C(17)-H(17)---F(2)	2.541	152.86
4	C(13)-H(13)--- π (Pyrrolic)	3.198	
5	π (Pyrrolic)---π (Pyrrolic)		

In the crystal structure packing of BODIPY **4a**, four mutual hydrogen bonding C(9)-H(9)---F(1) and C(9)-H(9)---F(2) interactions form a head to head pair. This pair connects to neighboring pair via C(7)-H(7)---*π* (Fc) and C(28)-H(28)---*π* (Phenyl) interactions forming a hydrogen bonded tetramer (Fig. 8). This tetramer further grows above and below via two mutual interactions C(10)-H(10)---F(2) to form a chain of tetramers, which further form a thick sheet via C(23)-H(23)---*π* (Fc) interaction (Fig. S19 (ESI)).

In the crystal structure packing of BODIPY **2d** the head to tail π---π staking between two BODIPY frameworks form a dimeric structure which is stabilized by C(17)-H(17)---F(2)

interaction. These dimeric structures extend into 1D chain via interaction C(13)-H(13)---π (Pyrrolic). The 1D chain further extends to complex 3D framework via interactions C(8)-H(8)---F(2) and C(1)-H(1)---F(1) (Fig. 9).

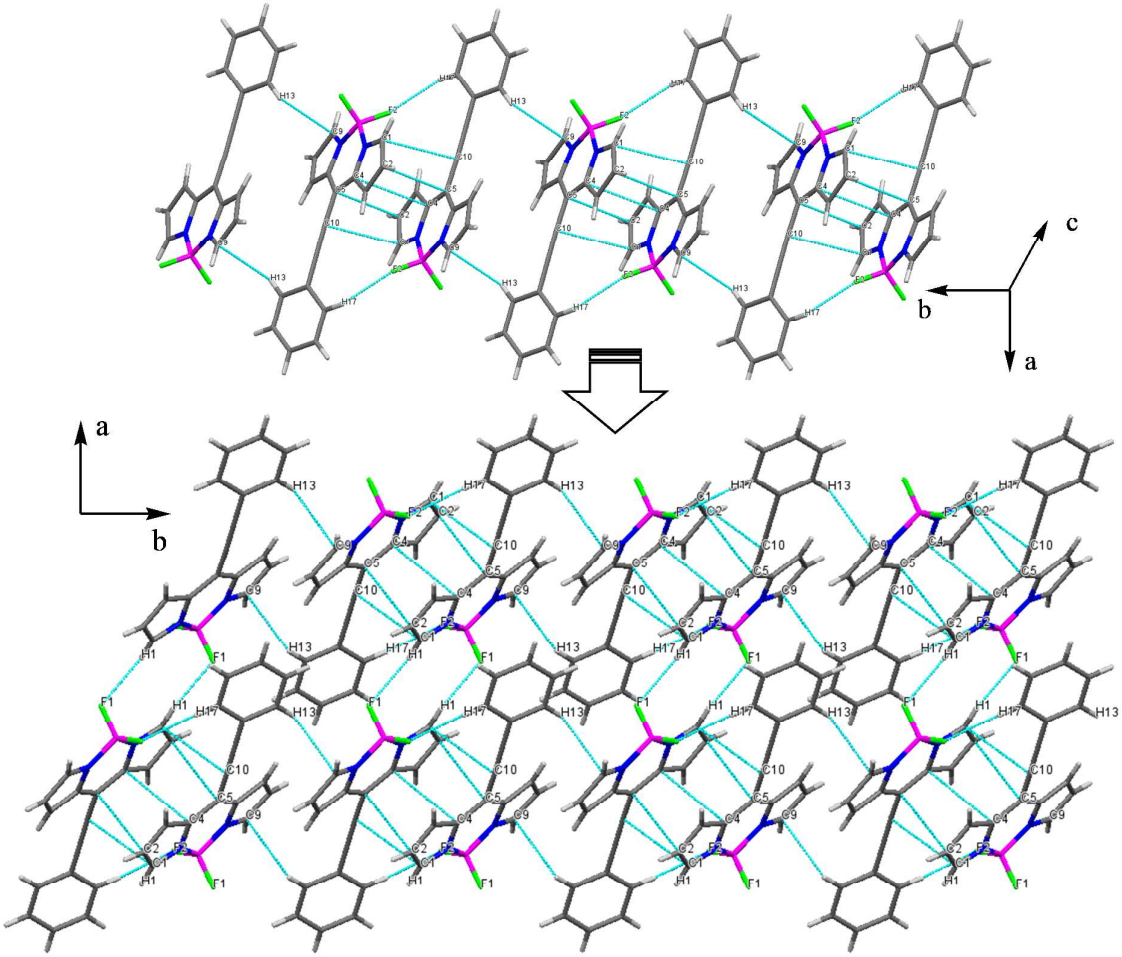

Fig. 9 Crystal structure packing of BODIPY **2d**.

Conclusions

We have developed a straightforward route for the synthesis of *meso* enyne substituted BODIPYs with two different substituents. The *meso* enyne substituted BODIPYs exhibit large Stokes shift, compared to the *meso* alkynylated BODIPYs. The electrochemical properties and theoretical calculations reveal strong donor-acceptor interactions between enyne substituent and the BODIPY. *Meso* enyne substituted BODIPYs with two different substituents are potential candidates for optoelectronic applications. This methodology would

enable rapid construction of a library of multi-substituted BODIPYs. The synthesis of new enyne substituted BODIPYs and their optoelectronic applications are ongoing in our group.

Experimental Section

Chemicals were used as received unless otherwise indicated. All oxygen or moisture sensitive reactions were performed under nitrogen/argon atmosphere using standard schlenk method. Triethylamine (TEA) was received from commercial source and distilled on KOH prior to use. ^{1}H NMR (400 MHz), and ^{13}C NMR (100 MHz) spectra were recorded on Bruker Avance (III) 400 MHz instrument using $CDCl_3$ as solvent. ^{1}H NMR chemical shifts are reported in parts per million (ppm) relative to the solvent residual peak ($CDCl_3$, 7.26 ppm). Multiplicities are given as: s (singlet), d (doublet), t (triplet), q (quartet), dd (doublet of doublets), m (multiplet), and the coupling constants, *J*, are given in Hz. ^{13}C NMR chemical shifts are reported relative to the solvent residual peak ($CDCl_3$, 77.36 ppm). HRMS were recorded on Bruker-Daltonics micrOTOF-Q II mass spectrometer. UV-visible absorption spectra of all compounds were recorded on Cary-100 Bio UV-visible Spectrophotometer and fluorescence spectra were recorded on Horiba Jobin Yvon Fluoromax 4P Spectrophotometers in toluene at the concentration of 0.1 optical densities at λ_{max}. The voltammograms were recorded on CHI620D electrochemical analyzer in dichloromethane solvent and 0.1 M $TBAF_6$ as supporting electrolyte. The electrodes used were glassy carbon as working electrode, Pt wire as counter electrode and the saturated calomel electrode as reference electrode. The potentials were referenced against Fc/Fc^{+} as per IUPAC guidelines.[12]

Generalized synthetic procedure for BODIPYs 2a, 2b, 3a and 3b (Method A)

8-Chloro BODIPY **1** (100 mg, 0.44 mmol), and corresponding arylethynes (**a** or **b**) (0.66 mmol) were dissolved in THF:triethylamine (10:1,v/v; 15 ml), and the mixture was cooled to 0 °C using an ice bath. The reaction mixture was purged with argon, and $Pd(PPh_3)_2Cl_2$ (15 mg, 5 mol%), and CuI (8.3 mg, 10 mol%) were added, followed by stirring at 0 °C for 30

min. The reaction mixture was brought to the room temperature and further stirred for 4 Hrs. After complete conversion of starting aryl alkyne **a/b**, the reaction mixture was evaporated to dryness, and the crude product was dissolved in CH_2Cl_2, chromatographed on silica (2:1; hexanes:CH_2Cl_2) to get **2a/2b** and **3a/3b**. The isolated products from column were recrystallized from chloroform: hexane (1:3) mixture as crystalline solid.

Generalized synthetic procedure for BODIPYs 3a, 3b, 4a, 4b and 4c (Method B)

Meso alkynylated BODIPY (**2a, 2b** or **2c**) (0.30 mmol) and aryl alkyne (ethynyl biphenyl, ethynyl naphthalene or ethynyl ferrocene) (0.30 mmol) were dissolved in THF:triethylamine (10:1,v/v; 15 ml). The reaction mixture was purged with argon, and $Pd(PPh_3)_2Cl_2$ (10.0 mg, 5 mol%), and CuI (6.7 mg, 10 mol%) were added, followed by stirring at room temperature for 10 Hrs. After completion of the reaction, the reaction mixture was evaporated to dryness, and the crude product was dissolved in CH_2Cl_2, chromatographed on silica (1:2; hexanes:CH_2Cl_2) to get **3a**, **3b**, **4a**, **4b** or **4c**. The isolated products from column chromatography were recrystallized from chloroform: hexane (1:3) mixture as crystalline solid.

Characterization Data

3a

Red crystalline solid. Yield: **Method A**- 20% (48 mg); **Method B**- 60 % (89 mg); ^{1}H NMR ($CDCl_3$, 400 MHz, ppm): δ 7.99-7.96 (m, 2H), 7.91 (bs, 2H), 7.76-7.73 (m, 2H), 7.69-7.66 (m, 2H), 7.58-7.55 (m, 2H), 7.53-7.50 (m, 3H), 7.48-7.45 (m, 4H), 7.44-7.41 (m, 2H), 7.40-7.34 (m, 2H), 7.33-7.30 (m, 2H), 6.55-7.53 (m, 2H); ^{13}C NMR ($CDCl_3$, 100 MHz, ppm): 144.0, 143.1, 142.8, 142.4, 140.4, 140.38, 136.4, 134.5, 133.3, 132.6, 130.1, 129.3, 129.2, 128.3, 128.2, 127.9, 127.8, 127.5, 127.4, 127.37, 125.4, 121.1, 118.3, 100.3, 87.4; ^{11}B NMR ($CDCl_3$, 128 MHz, ppm) 0.28 (t, $J_{B\text{-}F}$ = 28.7 Hz);; UV/vis (Toluene): λ_{max} (ε [$M^{-1}cm^{-1}$]) 515 (3.38×10^4). HRMS (ESI-TOF) m/z = calculated for $C_{37}H_{25}BF_2N_2$ = 585.1717 $[M+K]^+$, measured 585.1720 $[M+K]^+$.

4a

Purple-red crystalline solid. Yield: 61% (96 mg);. ^{1}H NMR ($CDCl_3$, 400 MHz, ppm): δ 7.93-7.90 (m, 4H), 7.74-7.70 (m, 2H), 7.68-7.65 (m, 2H), 7.51-7.48 (m, 2H), 7.43-7.39 (m, 4H), 6.57-6.55 (m, 2H), 4.27 (t, 2H, J = 1.76 Hz), 4.23 (t, 2H, J = 1.76 Hz), 4.08 (s, 5H); ^{13}C NMR ($CDCl_3$, 100 MHz, ppm): 143.7, 143.6,142.9,140.4, 136.5, 134.9, 133.8, 130.5, 129.3, 128.2, 127.8, 127.75, 127.4, 123.7, 118.1, 101.0, 83.4, 72.1, 70.5, 70.0, 63.7; ^{11}B NMR ($CDCl_3$, 128 MHz, ppm) 0.29 (t, $J_{B\text{-}F}$ = 29.5 Hz); UV/vis (Toluene): λ_{max} (ε [$M^{-1}cm^{-1}$]) 510 (3.4×10^4). HRMS (ESI-TOF) m/z = calculated for $C_{35}H_{25}BF_2FeN_2$ = 578.1429 $[M]^+$, measured 578.1425 $[M]^+$.

3b

Red crystalline solid. Yield: **Method A**- 21% (46 mg); **Method B**- 62 % (89 mg); ^{1}H NMR ($CDCl_3$, 400 MHz, ppm): δ 8.42 (s, 1H), 8.01-8.98 (m, 3H), 7.93-7.91 (m, 3H), 7.80-7.73 (m, 4H), 7.60-7.57 (m, 2H), 7.56 (s, 1H), 7.51-7.48 (m, 4H), 7.29-7.27 (m, 1H), 6.54-6.53 (m, 2H); ^{13}C NMR ($CDCl_3$, 100 MHz, ppm): 144.0, 143.0, 134.7, 134.6, 134.3, 133.8, 133.6, 133.5, 133.2, 132.8, 130.2, 129.1, 129.0, 128.5, 128.4, 128.3, 128.13, 128.1, 127.9, 127.7, 127.6, 127.3, 127.1, 126.1, 124.0, 119.6, 118.3, 101.0, 87.3; ^{11}B NMR ($CDCl_3$, 128 MHz, ppm) 0.34 (t, $J_{B\text{-}F}$ = 29.5 Hz); UV/vis (Toluene): λ_{max} (ε [$M^{-1}cm^{-1}$]) 515 (3.6×10^4). HRMS (ESI-TOF) m/z = calculated for $C_{33}H_{21}BF_2N_2$ = 517.1664 $[M+Na]^+$, measured 517.1651 $[M+Na]^+$.

4b

Purple crystalline solid. Yield: 60% (97 mg); ^{1}H NMR ($CDCl_3$, 400 MHz, ppm): δ 8.32 (s, 1H), 7.97-7.89 (m, 6H), 7.58-7.54 (m, 2H), 7.47 (s, 1H), 7.44 (d, 2H, J = 4 Hz), 6.57-6.56 (m, 2H), 4.30 (t, 2H, J = 1.76 Hz), 4.24 (t, 2H, J = 1.76 Hz), 4.09 (s, 5H); ^{13}C NMR ($CDCl_3$, 100 MHz, ppm): 143.8, 143.6, 134.9, 134.7, 134.2, 134.16, 133.5, 130.1, 129.1, 128.9, 128.1, 127.9, 127.6, 127.2, 124.3, 124.0, 118.2, 101.0, 83.39, 72.4, 70.9, 70.3, 53.8; ^{11}B NMR

($CDCl_3$, 128 MHz, ppm) 0.31 (t, J_{B-F} = 28.7 Hz); UV/vis (Toluene): λ_{max} (ε [$M^{-1}cm^{-1}$]) 510 (3.5×10^4). HRMS (ESI-TOF) m/z = calculated for $C_{33}H_{23}BF_2FeN_2$ = 575.1170 $[M+Na]^+$, measured 575.1170 $[M+Na]^+$.

4c

Purple crystalline solid. Yield: 58% (84 mg); ^1H NMR ($CDCl_3$, 400 MHz, ppm): δ 7.92 (s, 2H), 7.78-7.75 (m, 2H), 7.58-7.56 (m, 2H), 7.44 (d, 2H, *J* = Hz), 7.37 (s, 1H), 6.56-6.54 (m, 2H), 4.73 (t, 2H, *J* = 2 Hz), 4.41 (t, 2H, *J* = 1.76 Hz), 4.27 (multiplate, 2H), 4.23 (t, 2H, *J* = 1.76 Hz), 4.09-4.08 (m, 10 H); ^{13}C NMR ($CDCl_3$, 100 MHz, ppm): 143.9, 143.5, 142.2, 134.9, 134.7, 134.2, 132.2, 130.0, 127.4, 126.5, 122.8, 118.0, 84.3, 83.5, 72.1, 70.5, 70.2, 70.0, 69.9, 87.1, 63.8; UV/vis (Toluene): λ_{max} (ε [$M^{-1}cm^{-1}$]) 511 (3.7×10^4). HRMS (ESI-TOF) m/z = calculated for $C_{39}H_{29}BF_2Fe_2N_2$ = 686.1093 $[M]^+$, measured 686.1091 $[M]^+$.

Synthesis of BODIPY 2d

8-Chloro-BODIPY 1 (100mg 0.44 mmol) was dissolved in toluene and purged with argon. The (Phenylethynyl)tributylstannane reagent and $Pd(PPh_3)_4$ (25.5 mg, 5 mol%) were added, followed by reflux for 20 hrs under argon atmosphere. After completion of the reaction, the reaction mixture was evaporated to dryness, and the crude product was dissolved in CH_2Cl_2, chromatographed on silica (1:2; hexanes:CH_2Cl_2) to get BODIPY **2d**. The isolated product from column chromatography was recrystallized by slow evaporation of dichloromethane: hexane solution.

Product -Red crystalline solid. Yield: 80% (104 mg); ^1H NMR ($CDCl_3$, 400 MHz, ppm): δ 7.84 (s, 2H), 7.67 (d, 2H, *J* = 6.76 Hz), 7.55-7.45 (m, 3H), 7.41 (d, *J* = 4 Hz, 2H), 6.55 (d, *J* = 4 Hz, 2H); ^{13}C NMR ($CDCl_3$, 100 MHz, ppm): δ 143.6, 136.6, 132.8, 131.1, 129.2, 128.9, 127.3, 120.9, 118.4, 106.0, 84.1 ppm; HRMS (ESI-TOF) m/z = calculated for $C_{17}H_{11}BF_2N_2$ = 315.0879 $[M+Na]^+$, measured 315.0879 $[M+Na]^+$. Data in agreement with literature.[3h]

ASSOCIATED CONTENT

Supporting Information

† Electronic supplementary information (ESI) available: Photophysical and electrochemical characterization data, CCDC 1018403 – 1018405 for **2a**, **3b** and **4a** respectively and 1041639 for **2d**; copies of HRMS, ^{1}H, ^{13}C, ^{11}B and ^{19}B NMR spectra. This material is available free of charge via the internet at DOI: 10.1039/b000000x/

AUTHOR INFORMATION

Corresponding Author

* *Fax: +91 731 2361 482, E-mail: rajneeshmisra@iiti.ac.in*

ACKNOWLEDGMENT

We thank DST New Delhi for financial Support. BD and TJ thank CSIR and UGC New Delhi for their fellowships. We thank SIC, IIT Indore.

REFERENCES

1 (a) H. Lu, J. Mack, Y. Yang and Z. Shen, *Chem. Soc. Rev*., 2014, **43**, 4778–4823; (b) A. Loudet and K. Burgess, *Chem. Rev*., 2007, **107**, 4891–4932; (c) J. Han and K. Burgess, *Chem. Rev*., 2010, **110**, 2709-2728.

2 (a) A. Hagfeldt, G. Boschloo, L. C. Sun, L. Kloo, and H. Pettersson, *Chem. Rev.,* 2010, *110*, 6595–6663; (b) O. A. Bozdemir, R. Guliyev, O. Buyukcakir, S. Selcuk, S. Kolemen, G. Gulseren, T. Nalbantoglu, H. Boyaci and E. U. Akkaya, *J. Am. Chem. Soc.*, 2010, **132**, 8029; (c) W. Pang, X.-F. Zhang, J. Zhou, C. Yu, E. Hao, L. Jiao, *Chem. Commun.,* 2012, **48**, 5437-5439; (d) X.-F. Zhang, X. Yang, *J. Phys. Chem. B,* 2013, **117**, 9050-9055; (e) X.-F. Zhang, X. Yang, *J. Phys. Chem. B*, 2013, **117**, 5533-5539; (f) X.-F. Zhang, X. Yang, K. Niu, H. Geng, *J. Photochem. Photobiol. A: Chem.,* 2014, **285**, 16-20.

3 (a) A. B. Nepomnyashchii and A. J. Bard, *Acc. Chem. Res*., 2012, **45**, 1844-1853; (b) N. Boens, V. Leen and W. Dehaen, *Chem. Soc. Rev*., 2012, **41**, 1130-1172; (c) A. Bessette and G. S. Hanan, *Chem. Soc. Rev.,* 2014, **43**, 3342-3405; (d) G. Ulrich, R. Ziessel and A. Harriman, *Angew. Chem*., 2008, **120**, 1202-1219; *Angew. Chem. Int. Ed.,* 2008, **47**, 1184– 1201; (e) A. Wakamiya, T. Murakami and S.

Yamaguchi, *Chem. Sci.,* 2013, **4**, 1002; (f) M. Wada, S. Ito, H. Uno, T. Murashima, N. Ono, T. Urano and Y. Urano, *Tetrahedron Lett.*, 2001, **42**, 6711; (g) Z. Shen, H. Rohr, K. Rurack, H. Uno, M. Spieles, B. Schulz, G. Reck and N. Ono, *Chem.–Eur. J.*, 2004, **10**, 4853; (h) C. Yu, Y. Xu, L. Jiao, J. Zhou, Z. Wang, and E. Hao, *Chem.–Eur. J.*, 2012, **18**, 6437; (i) M. Nakamura, H. Tahara, K. Takahashi, T. Nagata, H. Uoyama, D. Kuzuhara, S. Mori, T. Okujima, H. Yamada and H. Uno, *Org. Biomol. Chem.,* 2012, **10**, 6840.

[4] (a) R. Misra, B. Dhokale, T. Jadhav and S. M. Mobin, *Dalton Trans.*, 2014, **43**, 4854; (b) X. Yang, X.-F. Zhang, X. Lu, C. Yu, L. Jiao, *J. Photochem. Photobiol. A: Chem.,* 2015, **297**, 39-44.

5 (a) B. Dhokale, P. Gautam, S. M. Mobin and R. Misra, *Dalton Trans.,* 2013, **42**, 1512-1518; (b) P. Gautam, B. Dhokale, S. M. Mobin and R. Misra, *RSC Adv.,* 2012, **2**, 12105-12107; (c) R. Misra, B. Dhokale, T. Jadhav and S. M. Mobin, *Dalton Trans.*, 2014, **43**, 4854. (d) R. Misra, B. Dhokale, T. Jadhav and S. M. Mobin, *Organometallics*, 2014, **33**, 1867–1877. (e) R. Misra, B. Dhokale, T. Jadhav and S. M. Mobin, *New J. Chem*. **2014**, *38*, 3579-3585. (f) R. Misra, T. Jadhav, B. Dhokale, P. Gautam, R. Sharma, R. Maragani and S. M. Mobin, *Dalton Trans.*, 2014, **43**, 13076-13086.

6 B. Dhokale, T. Jadhav, S. M. Mobin and R. Misra, *Chem. Commun.,* 2014, **50**, 9119-9121.

7 Y. Liu, M. Nishiura, Y. Wang, Z. Hou, *J. Am. Chem. Soc.,* 2006, **128**, 5592–5593.

8 (a) A. Carpita and A. Ribecai, *Tetrahedron Lett*., 2009, **50**, 204−207; (b) J. H. Olivier, F. Camerel, R. Ziessel, P. Retailleau, J. Amadou and C. Pham-Huu, *New J. Chem.,* 2008, **32**, 920−924; (c) L. Djakovitch, and P. Rollet, *Adv. Synth. Catal.,* 2004, **346**, 1782−1792.

9 (a) P. Arsenyan, K. Rubina, J. Vasiljeva and S. Belyakov, *Tetrahedron Lett.,* 2013, **54**, 6524−6528; (b) M. Pal, R. Dakarapu, K. Parasuraman, V. Subramanian and K. R. Yeleswarapu, *J. Org. Chem.,* 2005, **70**, 7179−7187. (c) Y. -J. Chen, G. -H. Lee, S. -M. Peng and C. Y. Yeh, *Tetrahedron Lett.,* 2005, **46**, 1541−1544; Corrigendum: *Tetrahedron Lett.,* 2005, **46**, 3265; (d) J. J. Gonzalez, A. Francesch, D. J. Cardenas and A. M. Echavarren, *J. Org. Chem.,* 1998, **63**, 2854−2857; (e) I. G. Stara, I. Stary, A. Kollarovic, E. Teply, D. Saman and P. Fiedler, *Tetrahedron,* 1998, **54**, 11209−11234; (f) Y. Liu, S. Jin, Z. Wang, L. Song and Y. Hu, *Org. Lett.,* 2014, **16**, 3524–3527.

10 (a) R. H. Platel and L. L. Schafer, *Chem. Commun.,* 2012, **48**, 10609-10611; (b) G. Midya, B. Parasar, K. Dharab and J. Dash, *Org. Biomol. Chem*., 2014, **12**, 1812; (c) S. D. Wobser, C. J. Stephenson, M. Delferro and T. J. Marks, *Organometallics,* 2013, **32**, 1317−1327.

11 H. Wang, M. G. H. Vicente, F. R. Fronczek, K. M. Smith, *Chem. Eur. J.* 2014, **20**, 5064−5074.

12 (a) N. K. Swamy, L. K. Tatini, J. M. Babu, P. Annamalai and M. Pal, *Chem. Commun.,* 2007, 1035-1037; (b) X. Zeng, *Chem. Rev.*, 2013, **113**, 6864−6900.

13 (a) U. Mayerhcffer, M. Gsanger, M. Stolte, B. Fimmel and F. Wurthner, *Chem. Eur. J.,* 2013, **19**, 218-232; (b) A. D. Laurent, C. Adamo and D. Jacquemin, *Phys. Chem. Chem. Phys.,* 2014, **16**, 14334-14356.

14 (a) B. Dhokale, P. Gautam and R. Misra, *Tetrahedron Lett.,* 2012*,* **53**, 2352-2354; (b) P. Gautam, B. Dhokale, V. Shukla, C. P. Singh, K. S. Bindra and R. Misra, *J. Photochem. Photobiol. A,* 2012, **239**, 24-27; (c) R. Misra, P. Gautam, R. Sharma and S. M. Mobin, *Tetrahedron Lett*., 2013, **54**, 381-383; (d) T. Jadhav, R. Maragani, R, Misra, V. Sreeramulu, D. N. Rao and S. M. Mobin, *Dalton Trans.,* 2013, **42**, 4340-4342; (e) R. Misra, P. Gautam, T. Jadhav and S. M. Mobin, *J. Org. Chem.,* 2013, **78**, 4940-4948; (f) R. Sharma, R. Maragani, S. M. Mobin and R. Misra, *RSC Adv.,* 2013, **3**, 5785; (g) R. Misra, T. Jadhav and S. M. Mobin, *Dalton Trans.,* 2013, **42**, 16614-16620. (h) R. Maragani and R. Misra, *Tetrahedron Lett*., 2013, **54**, 5399−5402; (i) R. Misra, T. Jadhav and S. M. Mobin, *Dalton Trans*., 2014, **43**, 2013-2022; (j) R. Misra, R. Sharma and S. M. Mobin, *Dalton Trans*., 2014, **43**, 6891-6896; (k) R. Misra, T. Jadhav, B. Dhokale and S. M. Mobin, *Chem. Commun*., 2014, **50**, 9076-9078; (l) V. A. Nadtochenko, N. N. Denisov, V. Y. Gak, N. V. Abramova, Loim, N. M. *Russ. Chem. Bull*., 1999, **48**, 1900; (m) S. Barlow and S. R. Marder, *Chem. Commun*., 2000, 1555-1562.

Table of Content

Meso enyne substituted BODIPYs: synthesis, structure and properties

Bhausaheb Dhokale, Thaksen Jadhav, Shaikh M. Mobin and Rajneesh Misra*.

Department of Chemistry, Indian Institute of Technology Indore,
IET-DAVV Campus, Khandwa Road, Indore 452 017 (India)
E-mail: rajneeshmisra@iiti.ac.in